Available online at www.sciencedirect.com
ScienceDirect
Physica A 379 (2007) 587–594
PHYSICA A
www.elsevier.com/locate/physa

Multicanonical sampling of vortex states in magnetic nanoelements

D. Reitzner[a], D. Horváth[b,*]

[a]Research Center for Quantum Information, Institute of Physics, Slovak Academy of Sciences, Dúbravská cesta 9, 845 11 Bratislava, Slovakia
[b]Department of Theoretical Physics and Astrophysics, Faculty of Science, P.J. Šafárik University, Park Angelinum 9, 041 54 Košice, Slovakia

Received 19 January 2007
Available online 21 February 2007

Abstract

An auto-adaptive multicanonical Monte Carlo (MMC) simulation method is suggested and tested on a single-vortex model of magnetic nanoelement. Simulation process consisting of nonequilibrium and equilibrium stages that circumvents ergodicity sampling problems which stem from a potential barrier standing between the vortex and counter-vortex states is proposed. The method is formulated by the means of an effective Hamiltonian with additional term proportional to the overlap of given configuration and bistable ground-state vortex configuration. The self-organized neural network is used to construct the synopsis of the vortex reversal process.

Keywords: Nanostructures; Magnetic vortex; Monte Carlo simulation; Neural-network classifier

1. Introduction

Single vortex magnetic configuration in nanoelements (Fig. 1) is a subject of theoretical [1,2] as well as experimental [3–7] studies. Elements of sub-100 nm dimensions are usually too small to support well-developed multi-domain structures, but they are too large for parallel alignment of spins. The magnetic vortex can be viewed as an intermediate state between the single-domain and multi-domain magnetic configurations. It exhibits decreased magnetostatic outer flow that can be exploited by designers of high-density information storage devices.

Every step towards miniaturization at micro-/nanoscales requires careful inclusion of thermal properties. The Monte Carlo method that has been exploited in bulk systems seems to be suitable also for purposes of nanoelements. The purpose of the present work is to present reliable simulation method that avoids difficulties with the quasi-ergodic violation [8]. From our experience, considering adaptivity principle may play a crucial role in methodology of the energy landscape exploration.

*Corresponding author.
E-mail address: horvath.denis@gmail.com (D. Horváth).

0378-4371/$ - see front matter
doi:10.1016/j.physa.2007.01.017

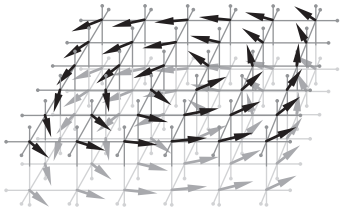

Fig. 1. The vortex ground state of 3D model of the magnetic nanoelement.

2. Monte Carlo simulation of magnetic nanoelement

The section introduces model of plate-shaped segment consisting of $N = 6 \times 6 \times 2$ cubic lattice sites of classical effective spin vectors $\mathbf{S}_i$, $\|\mathbf{S}_i\| = 1$. The magnetic contribution to the energy of element is described by the Hamiltonian

$$\mathscr{H} = -J \sum_{\langle i,j \rangle} \mathbf{S}_i \cdot \mathbf{S}_j + D \sum_{i \neq k}^{N \times N} \left[\frac{r_{ik}^2 \mathbf{S}_i \cdot \mathbf{S}_k - 3(\mathbf{S}_i \cdot \mathbf{r}_{ik})(\mathbf{S}_k \cdot \mathbf{r}_{ik})}{r_{ik}^5} \right] - B \sum_{i=1}^{N} (S_i^z)^2 , \tag{1}$$

where $\mathbf{r}_{ik}$ links ith and kth site. The first term proportional to J defines isotropic exchange coupling, where the summation symbolized by $\langle i,j \rangle$ is carried out over the nearest-neighbor sites. The second term of $\mathscr{H}$ is the dipolar coupling with summation over the $\frac{1}{2}N(N-1)$ spin pairs. In addition, the single-site uniaxial out-plane (z-axis) anisotropy proportional to parameter B is considered. As it can be demonstrated by simulated annealing method, for the parametric choice $D/J = 3 \times 10^{-3}$, $B/J = 0.1$ the ground state of element is the single vortex (see Fig. 1). Due to the center symmetry of element it is two-fold degenerated (bistable) with clockwise and counter-clockwise vorticity. Despite specific parameters chosen here, our results can be viewed in the light of scaling arguments [1,9] showing that class of equivalent samples exists that can be simulated using (relatively small number of) the effective spins.

2.1. The order parameter

An appropriate macroscopic characterization of nanoobjects with nontrivial configurations such as vortex represents a serious task. Here we suggest parameter which naturally corresponds to the geometry of given nanoelement. In analogy with ferromagnetic Ising-spin systems, where the order parameter (global magnetization) is defined as a projection onto two reference *attractors* (ground states), the *vorticity order parameter* of certain configuration $\mathscr{C} \equiv [\mathbf{S}_1, \mathbf{S}_2, \ldots, \mathbf{S}_N]$ is introduced as a projection

$$v(\mathscr{C}) = \frac{1}{N} \sum_{i=1}^{N} \mathbf{S}_i \cdot \mathbf{S}_i^{\mathrm{R}} \tag{2}$$

onto one of the two branches of the ground state $\mathscr{C}_{\mathrm{R}}^{\pm} \equiv [\pm\mathbf{S}_1^{\mathrm{R}}, \pm\mathbf{S}_2^{\mathrm{R}}, \ldots, \pm\mathbf{S}_N^{\mathrm{R}}]$. These configurations have been in our case obtained by simulated annealing method. For better readability the $\mathscr{C}$-dependence in $v(\mathscr{C})$ is omitted in below. In analogy to [10] we may now define the probability density function $\rho(v)$ of macroscopic vorticity v

$$\rho(v) = \frac{1}{\mathscr{Z}} \int_{\Omega} \mathrm{d}\{\mathscr{C}\} \delta(v - v(\mathscr{C})) \mathrm{e}^{-\beta\mathscr{H}} , \tag{3}$$

where δ is Dirac δ-function, β is the inverse temperature, $\mathscr{Z}$ is the partition function and integration is performed over the phase space Ω.

2.2. Preliminary qualitative considerations

The analysis of the quasi-static limit of the vortex reversal at finite temperatures is of the fundamental importance. We ask what intermediate states are met on the transition path from $v \simeq \pm 1$ to $v \simeq \mp 1$ and what are the properties of such transition. To answer this question the magnetic nanoelement has been repeatedly cooled down from sufficiently high temperatures. For temperatures $\beta J > 1$ the annealing has revealed (see

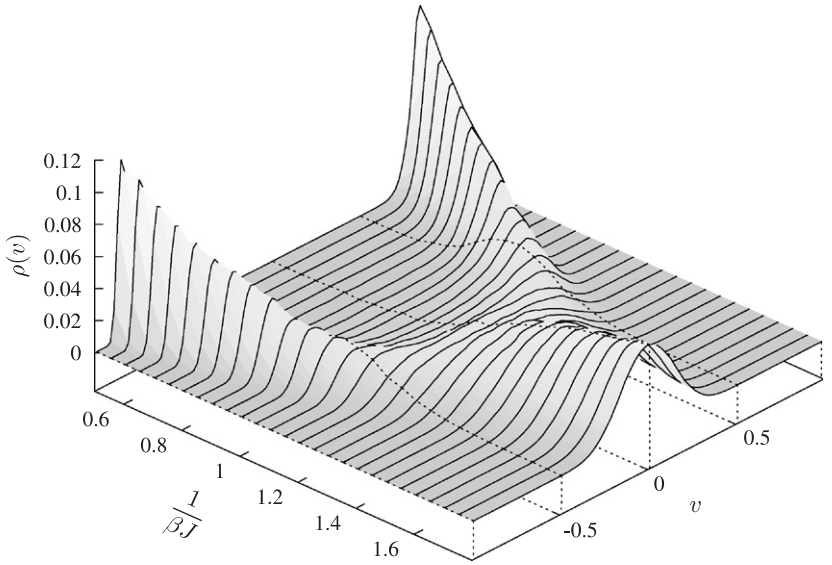

Fig. 2. The temperature dependence of the probability distribution function $\rho(v)$ normalized to $\int_{-1}^{1}\rho(v)\,\mathrm{d}v = 1$. The saddle between v and $-v$ is formed below $1/\beta J = 1$.

Fig. 2) broken symmetry between positive and negative v. It means that for low temperatures the transitions between v and $-v$ would be extremely rare. Quantitatively, with the energy of the ground state $\mathscr{H}|_{v=\pm1} = -192.66J$, the transition from $v = \pm1$ trough the point $v \simeq 0$ needs to overcome the energy barrier $E_{\mathrm{bar}} = \mathscr{H}_{v=\pm1} - \mathscr{H}_{v=0} \simeq 42J$. For $1/\beta = 0.3J$ the naïve application of Néel Brown formula provides probability estimate $\exp(-\beta E_{\mathrm{bar}}) \simeq 1.5 \times 10^{-61}$. The above probability estimation clearly implies that *canonical Monte Carlo* (CMC) with Metropolis single-spin moves included has to be inefficient for analysis of reversal. However, as it is well known, a broad theoretical framework for a more flexible sampling methodology is provided by general *multicanonical Monte Carlo* (MMC) [11].

3. Multicanonical sampling

MMC method has been originally suggested in connection with studies of the first order phase transitions where the jumps between phases are extremely rare. As it was demonstrated in the previous section, the same happens when considering vortex reversal problem. Although the MMC is quite general, the additional numerical work is needed to implement certain ingredients that allow sampling without ergodicity breaking.

The essence of MMC is a controlled non-Boltzmann weighing of the states which prefers those with former low occurrence probabilities. The weights are modified via effective Hamiltonian

$$\tilde{\mathscr{H}}(\mathscr{C}) = \mathscr{H}(\mathscr{C}) + \eta(v(\mathscr{C})), \tag{4}$$

where $\eta(v(\mathscr{C}))$ is an a priori unknown weight function. Using Eq. (4), multicanonical probability distribution function can be expressed as follows:

$$\rho_{\mathrm{MMC}}(v) = \frac{\mathscr{Z}}{\mathscr{Z}_{\mathrm{MMC}}}\,\mathrm{e}^{-\beta\eta(v)}\,\rho(v), \tag{5}$$

where $\mathscr{Z}_{\mathrm{MMC}}$ is multicanonical partition function. The utilization of MMC assembly is motivated by the need to sample states of different vorticity with nearly uniform distribution. However, any alternative sampling has to guarantee the uniqueness of averages. The MMC average $\langle Q\rangle_{\mathrm{MMC}}$ of a variable Q can be expressed using CMC average according to $\langle Q\rangle_{\mathrm{CMC}} = \langle Q\mathrm{e}^{-\beta\mathscr{H}}\rangle/\langle \mathrm{e}^{-\beta\mathscr{H}}\rangle$. When sampling with $\rho_{\mathrm{MMC}}(v)$ then

$$\langle Q\rangle = \frac{\langle Q\,\mathrm{e}^{-\beta\tilde{\mathscr{H}}+\beta\eta}\rangle}{\langle \mathrm{e}^{-\beta\tilde{\mathscr{H}}+\beta\eta}\rangle} = \frac{\langle Q\,\mathrm{e}^{\beta\eta}\rangle_{\mathrm{MCC}}}{\langle \mathrm{e}^{\beta\eta}\rangle_{\mathrm{MCC}}} \equiv \langle Q\rangle_{\mathrm{MMC}}. \tag{6}$$

When no ergodic problems occur for CMC there are no differences in both sampling methodologies. As Eq. (6) suggests the averages are equal within the statistical margin of error.

3.1. The auto-adaptive approach

In general, the methods of the construction of the weight function η are of the iterative nature [11]. The same holds for our approach that closely resembles that of Wang's and Landau's [12]. In our case the convergence to efficient weight function $\eta(v)$ is achieved with the help of histogram $H(v)$ counting the visits of vorticity intervals. This histogram is updated via rule

$$H_j^{(t+1)} = H_j^{(t)}(1 + u^{(t)}) \quad \text{if } v^{(t)} \in \langle v_j, v_{j+1}), \tag{7}$$

where $v_j = (2j - N_W - 2)/N_W, j = 1, 2, \ldots, N_W$ divides the vorticity space $I_v = \langle -1, 1\rangle$ into N_W sub-intervals. The sum $\mathcal{N}^{(t)} = \sum_{j=1}^{N_W} H_j^{(t)}$ is introduced to normalize the instant $H_j^{(t)}$ (see Eq. (8)). Quantity $u^{(t)} = u_0\, e^{-t/\tau}$ relaxes exponentially on the time scales of the order of adjustable parameter τ with t denoting number of MC steps. We have recognized numerically that including both factors in $H_j^{(t)}u^{(t)}$ improves the convergence. This modification is justified by supposition that vorticity regions frequently visited by sampling process are likely to be frequently visited also in further moves. The preliminary experimentation confirmed that considering $u^{(t)}$ without factor $H_j^{(t)}$ is not as efficient.

Each evaluation of the weight function is done according to

$$\eta^{(t)}(v) = \eta_0 \frac{H^{(t)}(v)}{\mathcal{N}^{(t)}}, \tag{8}$$

where η_0 is the proportionality factor that qualitatively corresponds to the largest energy barrier of the system; $H^{(t)}(v)$ is estimated by the linear interpolation between $H_j^{(t)}$ and $H_{j+1}^{(t)}$ with index

$$j \equiv \left[\frac{N_W(v+1)}{2} + 1\right]_{\text{int}}. \tag{9}$$

In our implementation we chose $\eta_0 = 500$ and $u_0 = 15$. The linear interpolation of $\eta^{(t)}(v)$ is needed since our trials indicate that discretized step-wise $\eta(v)$ contradicts to the continuity of the spin moves and strongly affects the transition probabilities.

The auto-adaptivity utilizes the interplay of $\mathcal{H}$ and $\eta(v)$ terms in $\tilde{\mathcal{H}}$, where weight function $\eta(v)$ is optimized to sample I_v efficiently. Since this requirement cannot be satisfied straightforwardly without numerical details that reflect the influence of original physical Hamiltonian $\mathcal{H}$, the rule Eq. (7) have to be applied. At the beginning of adaption, we choose $H_j^{(t=0)} = 1$ for each j and $\mathcal{N}^{(t=0)} = N_W$. For the transient regime the sampling is nonuniform with the preferred regions $v \sim \pm 1$. As the number of adaptive iterations increases (with η_0 properly chosen) the situation slowly alters because of the biased variations in $\eta(v)$ when the probability of jumps between vorticities of the opposite sign (see Fig. 3) rises. Finally, the exponential decrease of $u^{(t)}$ yields vanishing adaptive moves and thus fixation of $\eta(v)$.

3.1.1. Algorithm

Here we present some details of *single-spin-flip* MMC algorithm supplemented by the auto-adaptive process. The flowchart of the algorithm is specified as follows

I Initialization. Reset variables (simulation time $t = 0$), set $N_W = 100$, $H_j^{(t=0)} = 1$ and $\mathcal{N}^{(t=0)} = N_W$.

II Auto-adaptive nonequilibrium phase. Repeat the following (in our case 100 mil. MC steps):

(1) Pick random site i. The single spin $\mathbf{S}_i'^{(t)}$ of trial $\mathscr{C}'^{(t)}$ is treated according to:
- with probability 0.9 realize trial move $\mathbf{S}_i'^{(t)} = \mathbf{S}_i^{(t)} + \Delta\mathbf{S}^{(t)}$, where each component of the shift $\Delta\mathbf{S}^{(t)} = (\Delta S^x, \Delta S^y, \Delta S^z)$ is chosen uniformly from $\langle -0.3, 0.3\rangle$; $\mathbf{S}_i'^{(t)}$ is normalized to unity,
- with probability 0.1 the spin is reversed ($\mathbf{S}_i'^{(t)} = -\mathbf{S}_i^{(t)}$),

(2) Compute $\Delta\tilde{\mathcal{H}}^{(t)} = \tilde{\mathcal{H}}(\mathscr{C}'^{(t)}) - \tilde{\mathcal{H}}(\mathscr{C}^{(t)})$ via Eq. (8).

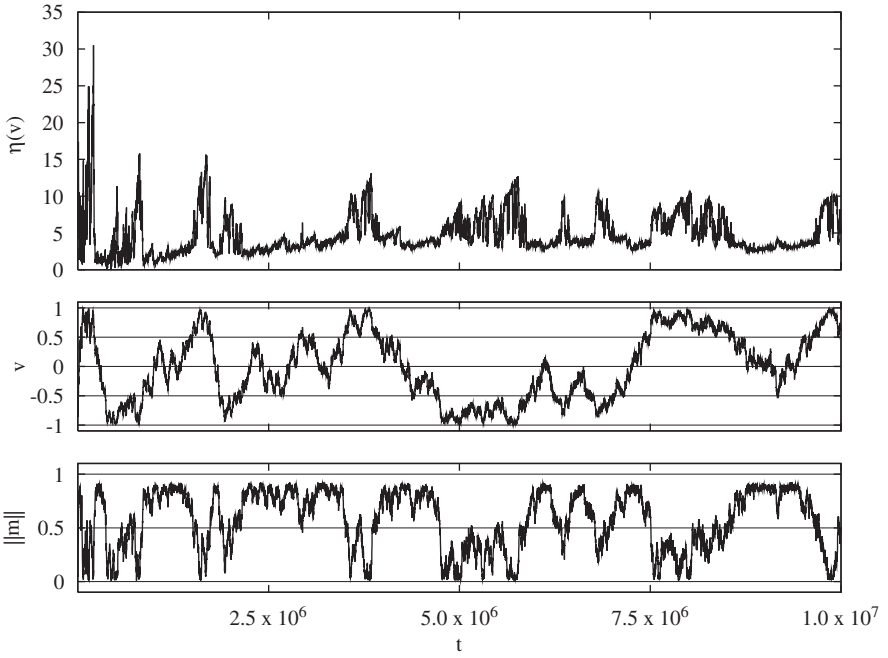

Fig. 3. The beginning of the auto-adaptive process of the weight function $\eta(v)$. The vicinity of $v \simeq 1$ is preferred until the weight function $\eta(v)$ is large enough for system to avoid this vorticity. The process, where the seemingly stabilized vorticity is eventually swapped by increasing weight function $\eta(v)$, is repeated several times until $\eta(v)$ is adapted. In further these data were plotted in the form of Fig. 5. We see that for high $|v|$ the magnetization is low. On the other hand any decrease of $|v|$ is coupled to the $\|\mathbf{m}\|$ increase. The coupling can be interpolated by Eq. (12).

(3) Accept the alternatives from (1) with probability $\min\left\{1, \mathrm{e}^{-\beta\Delta\tilde{\mathscr{H}}^{(t)}}\right\}$:
   (a) Update $\mathbf{S}_i^{(t)}$ by auxiliary $\mathbf{S}_i^{(t+1)} = \mathbf{S}'^{(t)}_i$.
   (b) Compute v for $\mathscr{C}'^{(t)}$ using Eq. (2).
(4) Determine j corresponding to v using Eq. (9), update $H_j^{(t)}$ and $\mathscr{N}^{(t)}$ according to Eq. (7).

III Equilibrium data accumulation.

(1) Record data for repeated steps (1)–(3) from phase II for $\eta(v^{(t+1)})$ fixed by step II (4).
(2) Calculate averages of interest using Eq. (6).

4. Results

Here we mention several results interesting from both physical and also computational point of view. Firstly, in Fig. 3 we checked that the algorithm significantly improves ergodicity of sampling within the vorticity space. It shows that no vorticity region has been ignored. Due to the stochastic nature of process the form of the weight function $\eta(v)$ is not strictly symmetric. However, from the theory we know that the symmetry of $\mathscr{H}$ with respect to $\mathbf{S}_i \to -\mathbf{S}_i$ implies the symmetry $\eta(v) = \eta(-v)$.[1] Since the numerical output does not strictly provide even $\eta(v)$, further simulations can be accelerated by using interpolation that utilizes even Chebyshev polynomials (see Fig. 4).

$$\eta(v) \simeq \sum_{k=0}^{13} a_{2k} \Phi_{2k}(v), \tag{10}$$

where $\Phi_{2k}(v) = \cos(2k \operatorname{accros} v)$. The coefficients a_{2k}, $k = 0, 1, \ldots, 13$ are obtained by fitting. Due to the limited space, only two of them $a_0 = (1.05 \pm 0.01) \times 10^{-2}$, $a_2 = (2.95 \pm 0.22) \times 10^{-3}$ are listed here.

[1] Let us note that nonsymmetric modes induced by the spin single-site defects were also investigated and tested with success.

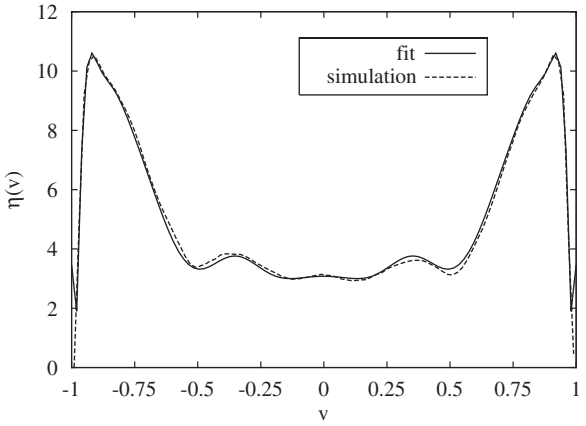

Fig. 4. The nonsymmetric weight function $\eta(v)$ obtained from simulation (dashed line) compared with its symmetric approximation by the series of even Chebyshev polynomials (full line).

Table 1
The comparison of averages corresponding to CMC and MMC sampling schemes obtained by simulations at temperature $\beta J = 1/0.3$

Sampling	$\langle \|\mathbf{m}_1\|^2 \rangle$	$\langle \|\mathbf{m}_2\|^2 \rangle$	$\langle \mathscr{H} \rangle$	$\langle \|\mathbf{m}\|^2 \rangle$
MMC	0.368	0.365	−170.08	0.0108
CMC	0.369	0.369	−170.09	0.0105

To demonstrate the justness of the proposed algorithm we have checked that averages invariant to $v \to -v$ exhibit equivalence between MMC and CMC (see Table 1). Namely, these averages are not affected by quasi-ergodic violation. The examples are internal energy $\langle \mathscr{H} \rangle$ and magnetization

$$\mathbf{m} = \frac{1}{N} \sum_{i=1}^{N} \mathbf{S}_i \tag{11}$$

which, when confronted (see Table 1), do not expose relevant differences. More detailed test is provided by averages of the magnetic moments $\mathbf{m}_1$ and $\mathbf{m}_2$ of the nanoelement halves. Also in this case the tests support validity of our MMC implementation.

4.1. The vorticity reversal

The exceptionalities of stochastic reversal are plotted in Fig. 3, where the time dependencies of magnetization amplitude and vorticity are plotted. We see that absolute vorticity $|v|$ is statistically coupled with the $\|\mathbf{m}\|$. These correlations can be interpolated quantitatively by the quadratic "equation of state"

$$\langle \|\mathbf{m}\| \rangle \simeq b_0 v^2 + b_1 \tag{12}$$

with coefficients $b_0 = -0.954$ and $b_1 = 0.873$ obtained by fitting (Fig. 5).

The visual inspection of the vorticity reversal as well as previous results (see Eq. (12)) reveal that the configurations are ordered and queued in a non-random fashion. We can suppose that these ordered configurations composing vorticity reversal paths are attractors on the energy landscape. This view hints on the use of adaptive classifying systems. Particular solution of such data processing problem that we exploited is offered by the concept of artificial neural networks—*adaptive resonance theory* (ART) [13]. This concept is suitable for our purposes since in Ref. [14] it was demonstrated that the unsupervised ART classifier applied to

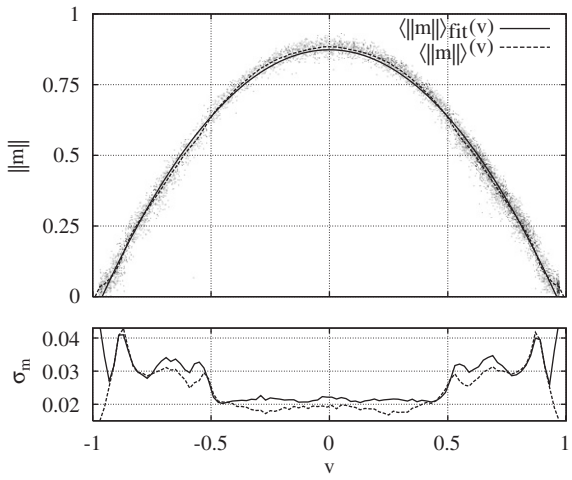

Fig. 5. The dependence of the mean amplitude of magnetization $\langle\|\mathbf{m}\|\rangle$ on the vorticity (dashed line) compared to its quadratic fit (full line) Eq. (12). The additional information about the local validity of quadratic interpolation and the mean amplitude of magnetization is provided by the bottom figure showing the v-dependence of dispersion $\sigma_{\mathbf{m}} = \sqrt{\langle(\|\mathbf{m}\| - \langle\|\mathbf{m}\|\rangle)^2\rangle}$. Small dots belong to states gathered by stochastic dynamics.

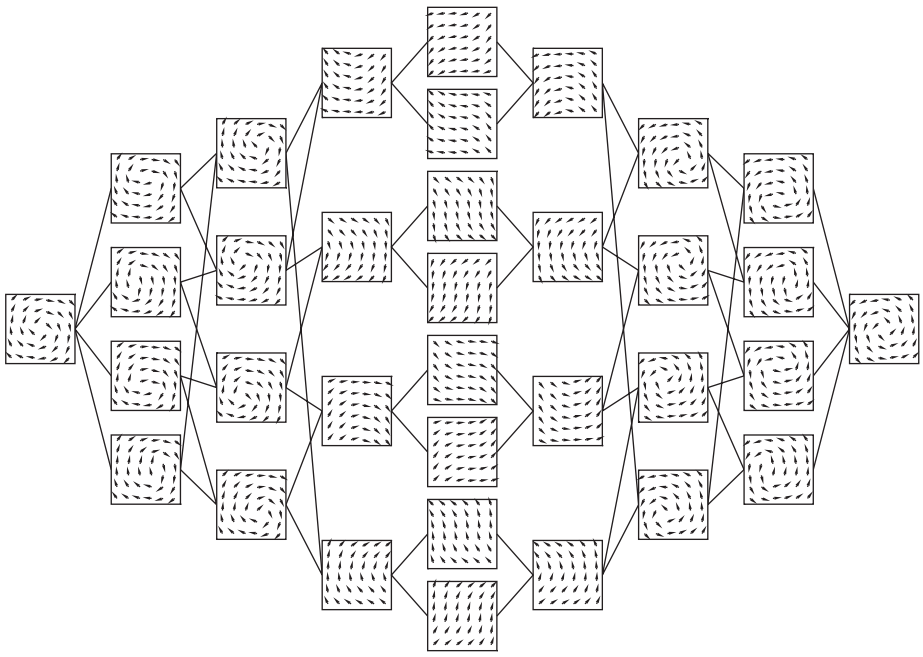

Fig. 6. Most probable paths of the vortex reversal obtained by MMC sampling with outputs reduced by the ART network. The reversal nucleates by developing a deviation of the vortex core. The proceeding states are: U → S → U (axially symmetric) → counter-vortex. The S states belong to $v \simeq 0$.

magnetic system is capable of selecting representative configurations (RCs) of a given nanoelement. In this context it should be mentioned that a similar approach [15] has been used to magnetic force microscopy images of thin film media.

In the present approach the ART network had been trained and stabilized at 47 neurons (each neuron encodes one RC). Since the adaptation acts in a probabilistic manner, the stored RCs had to be post processed

to suppress the noise level. This was achieved by a simulated annealing process starting at low temperatures. Resulting meta-stable RCs were supplemented by their corresponding symmetric counterparts (see Fig. 6).

RCs generated in such way have been used in classification of the states generated by the MMC simulation. The output of this detailed Markovian chain of spin configurations has been coarse-grained using the mapping: $\mathscr{C}$ to RCs. For given $\mathscr{C}$ the mapping consists of selecting an exceptional RC that yields the maximum mutual overlap. The reduced path consisting of RCs has been analyzed and the transition probabilities between the connected pairs of RCs have been evaluated. The synopsis of the most probable path is depicted in Fig. 6. It shows that $v \to -v$ process nucleates via the disturbance of the position of the vortex core. Subsequently, the transition (U state) $\to$ (S state) $\to$ (U axially symmetric to the proceeding one) follows. The final stage is the counter-vortex. Its core is formed at the corners of the nanoelement.

5. Conclusion

The simulations of square magnetic nanoelement state have been carried out via the MMC method. The scalar parameter characterizing the vortex state has been constructed via numerical optimization. The same characteristics have been used to perform the auto-adaptive construction of the effective Hamiltonian that admits more efficient sampling. It was demonstrated that the method enhances the frequency of transitions between opposite vorticities. Finally, the coarse-grained paths of vorticity reversal have been constructed by the methodology of ART networks.

Acknowledgments

The authors would like to express their thanks to Slovak Grant agency VEGA (Grant No.1/2009/05) and Grant agency APVT-51-052702 for financial support.

References

[1] E.Yu. Vedmedenko, A. Ghazali, Phys. Rev. B 59 (1999) 3329.
[2] K.Yu. Guslienko, K.L. Metlov, Phys. Rev. B 63 (2001) 100403.
[3] T. Shinjo, T. Okuno, R. Hassdorf, K. Shigeto, T. Ono, Science 289 (2000) 930.
[4] J. Raabe, R. Pulwey, R. Sattler, T. Schweinböck, J. Zweck, D. Weiss, J. Appl. Phys. 88 (2000) 4437.
[5] V. Novosad, M. Grimsditch, K.Yu. Guslienko, P. Vavassori, Y. Otani, S.D. Bader, Phys. Rev. B 66 (2002) 052407.
[6] T. Uhlig, M. Rahm, Ch. Dietrich, R. Höllinger, M. Heumann, D. Weiss, J. Zweck, Phys. Rev. Lett. 95 (2005) 237205.
[7] J.P. Park, P.A. Crowell, arXiv: cond-mat/0508597.
[8] K. Binder, D.W. Heermann, Monte Carlo Simulation in Statistical Physics, Springer, Berlin, Heidelberg, 2002.
[9] J. d'Albuquerque e Castro, D. Altbir, J.D. Retamal, P. Vargas, Phys. Rev. Lett. 88 (2002) 237202-1.
[10] N. Wilding, D.P. Landau, Monte Carlo methods for bridging timescale gap, in: P. Nielaba, M. Mareschal, G. Ciccoti (Eds.), Bridging Time Scales, Molecular Simulations for the Next Decade, Springer, Berlis, 2002, p. 231.
[11] B.A. Berg, U. Hansmann, T. Neuhaus, Z. Phys. B 90 (1993) 229;
B.A. Berg, Comput. Phys. Commun. 104 (2002) 52.
[12] F. Wang, D.P. Landau, Phys. Rev. Lett. 86 (2001) 2050.
[13] L. Fausett, Fundamentals of Neural Networks, Prentice-Hall, Engelwood Clipp, NJ, 1994; G.A. Carpenter, S. Grossberg, Pattern Recognition by Self-Organizing Neural Network, MIT Press, Cambridge, MA, 1991.
[14] M. Gmitra, D. Horváth, J. Magn. Magn. Mater. 265 (2003) 69;
M. Gmitra, D. Horváth, D. Reitzner, Czech. J. Phys. 54 (2004) D631.
[15] H.V. Jones, R.W. Chantrell, J. Appl. Phys. 91 (2002) 8855.